Research Square

Preprints are preliminary reports that have not undergone peer review.
They should not be considered conclusive, used to inform clinical practice,
or referenced by the media as validated information.

Transverse Distribution of the Streamwise Velocity for the Open-channel Flow With Floating Vegetated Islands

Xuecheng Fu
Wuhan University
Feifei Wang
Wuhan University
Mengyang Liu
Wuhan University
Wenxin Huai (wxhuai@whu.edu.cn)
wuhan university

Research Article

Keywords: Floating vegetated island, Depth-averaged streamwise velocity, Velocity distribution, Secondary flow, Comprehensive friction factor, Drag force term

Posted Date: February 8th, 2021

DOI: https://doi.org/10.21203/rs.3.rs-165125/v1

License: This work is licensed under a Creative Commons Attribution 4.0 International License.
Read Full License

Transverse distribution of the streamwise velocity for the open-channel flow with floating vegetated islands

Xuecheng Fu[1], Feifei Wang[1], Mengyang Liu[1], Wenxin Huai[1,*]

[1] *State Key Laboratory of Water Resources and Hydropower Engineering Science, Wuhan University, Wuhan, Hubei 430072, China*

E-mail Addresses:

Xuecheng Fu, xuechengfu@whu.edu.cn;

Feifei Wang, ffwang1991@whu.edu.cn;

Mengyang Liu, liumy@whu.edu.cn;

Wenxin Huai, *Corresponding author, wxhuai@whu.edu.cn.

Abstract

Floating vegetation islands (FVIs) have been widely utilized in various river ecological restoration projects due to their ability to purify pollutants. FVIs float at the surface of shallow pools with their roots unanchored in the sediment. Biofilm formed by roots under islands filters nutrients and particles in the water flowing through it. Flow field disturbance will occur and transverse distribution of flow velocity will change due to the existence of FVIs. Transport efficiency of suspended solids, nutrients, and pollutants will also be altered. A modified analytical model that considers effects of boundary friction, drag force of vegetation, transverse shear turbulence, and secondary flow is established to predict transverse variation of depth-averaged streamwise velocity for the open-channel flow with FVIs using Shiono and Knight method. The simulation results with suitable boundary conditions successfully predicted lateral profile of the depth-averaged streamwise velocity compared with the experimental results of symmetrical and unsymmetrical arrangements of FVIs. Hence, the presented model can provide guidance for investigating flow characteristics of rivers with FVIs.

Keywords: Floating vegetated island · Depth-averaged streamwise velocity · Velocity distribution · Secondary flow · Comprehensive friction factor · Drag force term

Highlights

An analytical model of depth-averaged streamwise velocity for open-channel flow with floating vegetated islands is proposed.

The modeled results indicate good predictions in depth-averaged streamwise velocity.

The new calculation method of comprehensive friction factor is derived.

Introduction

Floating vegetation islands (FVIs) are widely used in river ecosystem recovery projects due to their satisfactory pollutant purification ability. Roots of floating macrophytes on the surface of shallow pools are unanchored in the sediment (Nahlik and Mitsch 2006; Downing–Kunz and Stacey 2011). The root system extends down to the river bottom and provides for the matrix in the formation of biofilm with its ability to remove small suspended particles, dissolved pollutants, and nutrients (Billore and Sharma 2009; Hwang and LePage 2011; Tanner and Headley 2011; Chua et al. 2012; Liu et al. 2019). The existence of FVIs remarkably alters the internal structure of fluid, increases the complexity of the flow pattern (Yang et al. 2007), and impacts the transport and diffusion of pollutants and sediment transfer (Huai and Li 2016). Specifically, FVIs directly affect the surface of the fluid by reducing the flow velocity in this area. The vertical distribution of the streamwise velocity is altered and the maximum velocity appears in the middle water depth rather than the water surface under the joint action of FVIs and rough flume bed unlike the open-channel flow. However, flow characteristics of the open-channel flow with FVIs are similar to those of ice-covered channels. Therefore, investigating flow characteristics of the open-channel flow with FVIs, such as velocity distribution, flow rate, and secondary currents, is necessary.

The depth-averaged streamwise velocity of natural streams should be predicted first to explore the sediment transport and river evolution (Bonakdari 2012; Liu et al. 2013a), and the total rate of flow can then be obtained by integrating the depth-averaged streamwise velocity over the cross section. The transverse distribution of the streamwise velocity in the open channel with FVIs can be acquired according to the depth-averaged Navier–Stokes (N–S) equation. Shiono and Knight (1991) initially derived the depth-averaged form of the N–S equation in the compound channel. The majority of studies on the transverse distribution of the streamwise velocity in the channel have focused on the flow through submerged and

emergent canopies, typically introduced the term of vegetation drag force into the N–S equation while considering the effect of the canopy, and applied different methods to improve the model. For instance, Chen (2010) and Huai (2011) derived a nondimensional form of the N–S equation to overcome limitations caused by the dimensional one and quantify the effects of gravity and friction. A certain number of subregions in the transverse direction were defined with different parameters in each subregion on the basis of mixing layer theory (White and Nepf 2008; Huai et al. 2013; Liu et al. 2013b; Fernandes et al. 2014). Modified calculation methods of unknown coefficients, such as friction, eddy viscosity, and secondary flow coefficients, are put forward to improve the reliability of the calculation results (Rameshwaran and Shiono 2007; Huai et al. 2008; Huai et al. 2009; Devi and Khatua 2016). Meanwhile, some studies have focused on the ice-covered channel flow because its flow characteristics are similar to those of the channel flow with FVIs to some extent. Zhong (2019) and Wang (2020) investigated the transverse distribution of the depth-averaged streamwise velocity in the rectangular flume and the compound channel according to a two-layer hypothesis, respectively. However, studies concentrating on the transverse distribution of the depth-averaged streamwise velocity of the open-channel flow with FVIs are limited.

Accordingly, an analytical model derived from the Shiono and Knight method (SKM) (Shiono and Knight 1991) and secondary flow theory (Ervine et al. 2000) for predicting the transverse distribution of the depth-averaged streamwise velocity in the open channel with FVIs is proposed in this study. Canopy resistance is added to the N–S equation that considers the existence of FVIs, and the analytical solution of the depth-averaged streamwise velocity is obtained by solving the governing equation. The analytical solution is then compared with experimental data acquired from symmetrical and unsymmetrical arrangements of FVIs. The consistency of the modeled results with experimental data proves the reasonability and validity of the analytical model. Meanwhile, the analytical model can provide a reference for investigating flow characteristics of the open channel with FVIs.

Experimental setup

Two experimental conditions, namely, symmetrical and asymmetrical arrangements of FVIs, are carried out in the laboratory, as illustrated in Fig. 1, and their corresponding series of cases are illustrated in Fig. 2. Specifically, the experiment was conducted in a 20 m-long and 1 m-wide (B) glass flume with a bed slope S_0 equal to 0.01%. FVIs with widths of 0.6 and 0.3 m (b) are arranged symmetrically along the center with lengths of 5 and 8 m, respectively, while its unsymmetrical counterpart with a respective width and length of 0.3 (b)

and 8 m is set close to the shore wall. Moreover, steady and uniform flow is adopted in these cases. The water depth is adjusted using a tailgate with the discharge regulated by an electromagnetic flowmeter installed upstream of the channel, and the point velocity is measured with a SonTek 3D Acoustic Doppler Velocimeter (ADV). The root system of floating vegetation is simulated using a series of rigid columns. Columns are orthogonally aligned with the side length of the square element equal to 0.05 m. The canopy height and diameter are h_c = 0.25 m and D = 0.006 m, respectively. Columns are vertically attached to several suspended polyvinyl chloride (PVC) plates. The channel bed is covered with some 2 m-long, 1 m-wide, and 0.01 m-thick PVC base plates.

(a) Asymmetrical arrangement case (b) Symmetrical arrangement case

Fig. 1 Global view of the channel with different FVI arrangements

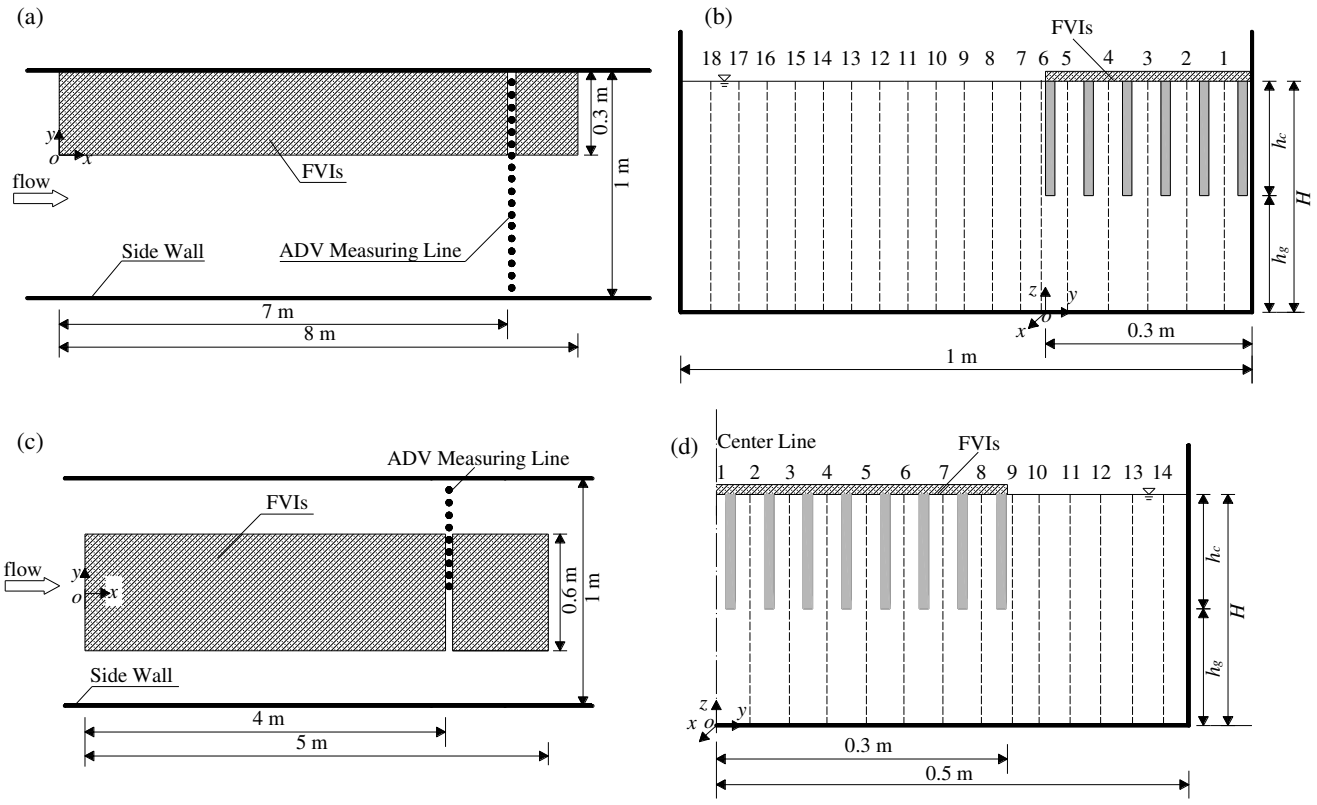

Fig. 2 Diagrams of the FVI layout in the laboratory flume: (a) Top view of the asymmetrical arrangement case; (b) Cross-section profile of the asymmetrical arrangement case; (c) Top view of the symmetrical arrangement case; (d) Cross-section profile of the symmetrical arrangement case with the canopy height h_c, gap height h_g, and water depth H

The entire cross section of the unsymmetrical arrangement of FVIs is considered for analysis, while half of the channel is analyzed for symmetrical case on account of its symmetry. Fig. 2 shows the diagrams of unsymmetrical and symmetrical cases, including top views and cross-sectional drawings. The measuring section is set 1 m away from the end of FVIs. Fourteen to eighteen measuring lines are taken in the cross-sectional direction according to different arrangement cases. Seventeen to twenty-two measuring points are selected for each perpendicular with a measuring spacing of 0.02–0.04 m to improve the accuracy of the vertical velocity distribution. Instantaneous velocities are obtained using the ADV at a frequency of 50 Hz with a sampling period of 160 s. High-quality measuring data are then conserved by removing low signal-to-noise ratio (<15 dB) and low-correlation (<70%) samples. Water depths of 0.43 and 0.48 m are adopted under these working conditions. Experimental parameters are listed in Table 1.

Table 1

Geometric and hydraulic parameters of experiments

Cases	FVI layout	Q (m^3/s)	H (m)	h_c (m)	h_g (m)	b (m)	B (m)	S_0 (%)
Run 1	Symmetric arrangement	0.0420	0.43	0.25	0.18	0.6	1.0	0.01
Run 2	Symmetric arrangement	0.0469	0.48	0.25	0.23	0.6	1.0	0.01
Run 3	Symmetric arrangement	0.0423	0.43	0.25	0.18	0.3	1.0	0.01
Run 4	Symmetric arrangement	0.0475	0.48	0.25	0.23	0.3	1.0	0.01
Run 5	Asymmetric arrangement	0.0424	0.43	0.25	0.18	0.3	1.0	0.01
Run 6	Asymmetric arrangement	0.0477	0.48	0.25	0.23	0.3	1.0	0.01

Theoretical analysis

Deriving the depth-averaged streamwise momentum equation with additional canopy resistance is necessary to predict the transverse variation of the depth-averaged streamwise velocity of the open-channel flow with FVIs. By introducing the canopy resistance into the Navier-Stokes equation and combining it with the continuity equation, the governing equation can be obtained as follows (Shiono and Knight 1991):

$$\rho[\frac{\partial UV}{\partial y}+\frac{\partial UW}{\partial z}]=\rho g S_0+\frac{\partial \tau_{yx}}{\partial y}+\frac{\partial \tau_{zx}}{\partial z}-F_v, \quad (1)$$

where x, y, and z represent streamwise, transverse, and vertical coordinates, respectively; U, V, and W are time-averaged velocities in {x, y, z} directions; ρ denotes the water density; S_0 is the channel bed slope; g represents the gravitational acceleration; τ_{zx} and τ_{yx} denote the Reynolds shear stresses on planes perpendicular to z and y directions, respectively, $\tau_{zx}=-\rho\overline{u'w'}$ and $\tau_{yx}=-\rho\overline{u'v'}$; u', v', and w' are fluctuating velocities in {x, y, z} directions. The overbar indicates that parameters are averaged over time. F_v is the drag force generated by the canopy per unit fluid volume, which can be expressed as

$$F_v=\frac{1}{2}\rho(C_d\beta A_v)U^2, \quad (2)$$

where C_d denotes the vegetation drag coefficient; β represents the shape factor of the canopy; and A_v is the projected area of canopy per unit volume in the longitudinal direction, $A_v = mD$ = 2.4 m^{-1} and m represents the number of columns per bed area (Nepf and Vivoni 2000).

The depth-averaged momentum equation is obtained by integrating Eq. (1) over the water depth H. Assuming that $W(0) = W(H) = 0$, we have

$$\rho \frac{\partial H(UV)_d}{\partial y} = \rho g H S_0 + \frac{\partial H \bar{\tau}_{yx}}{\partial y} - \tau_d - \int_0^H \frac{1}{2}\rho(C_d \beta A_v) U^2 dz, \quad (3)$$

where $(UV)_d = \frac{1}{H}\int_0^H UV dz$; $\bar{\tau}_{yx}$ denotes the depth-averaged Reynolds shear stress on the plane perpendicular to the y-direction, $\bar{\tau}_{yx} = \frac{1}{H}\int_0^H (-\rho\overline{u'v'})dz$; and τ_d represents the comprehensive boundary shear stress, $\tau_d = -\int_0^H \frac{\partial \tau_{zx}}{\partial z} dz$. The integral of the canopy resistance term over the water depth H can be divided into two parts, namely, 0–h_g and h_g–H. Assuming that the canopy resistance term in the 0–h_g region is equal to zero, the integral of the canopy resistance term can be expressed as

$$\int_0^H \frac{1}{2}\rho(C_d \beta A_v) U^2 dz = \int_{h_g}^H \frac{1}{2}\rho(C_d \beta A_v) U^2 dz = \frac{1}{2}\rho(C_d \beta A_v) h_c U_{d_c}^2, \quad (4)$$

where h_g is the height of the gap region; h_c is the height of the canopy region, $h_c = H - h_g$; and U_{d_c} is the depth-averaged streamwise velocity in the canopy region, $U_{d_c} = \frac{1}{h_c}\int_{h_g}^H U dz$. The relationship between the depth-averaged streamwise velocity in the canopy region and the depth-averaged streamwise velocity of the total water depth H presented in Plew (2011) is expressed as follows:

$$\frac{U_{d_c}}{U_d} = \frac{-\alpha^2 - C_b h^2 + (1-h)\sqrt{Ah(1-h)(C_b h + \alpha^2) - \alpha^2 C_b h}}{Ah(1-h)^3 - \alpha^2 - C_b h^3} = P_u, \quad (5)$$

where U_d is the depth-averaged streamwise velocity, $U_d = \frac{1}{H}\int_0^H U dz$; $h = h_c / H$; α is a dimensionless parameter, $\alpha^2 = <u'w'>_c / (U_{d_g} - U_{d_c})^2$; U_{d_g} is the depth-averaged streamwise velocity in the gap region, $U_{d_g} = \frac{1}{h_g}\int_0^{h_g} U dz$; $<u'w'>_c$ is the shear stress at the bottom of the canopy; C_b is the bed friction coefficient; and $A = \overline{C_d A_v} H / 2$, and the overbar of $\overline{C_d A_v}$ shows that the vegetation drag coefficient and projected area of vegetation are multiplied and then averaged vertically.

Eqs. (4) and (5) are substituted into Eq. (3) to obtain the following:

$$\rho\frac{\partial H(UV)_d}{\partial y}=\rho gHS_0+\frac{\partial H\bar{\tau}_{yx}}{\partial y}-\tau_d-\frac{1}{2}\rho(C_d\beta A_v)h_c P_u^2 U_d^2, \tag{6}$$

The eddy viscosity method is widely used in numerical simulation. Hence, $\bar{\tau}_{yx}$ can be expressed as follows (Shiono and Knight 1991):

$$\bar{\tau}_{yx}=\rho\bar{\varepsilon}_{yx}\frac{\partial U_d}{\partial y} \tag{7}$$

where $\bar{\varepsilon}_{yx}$ denotes the depth-averaged eddy viscosity, $\bar{\varepsilon}_{yx}=\lambda HU_*$; λ represents the dimensionless eddy viscosity; and U_* denotes the local shear velocity, $U_*=\sqrt{\tau_d/\rho}=\sqrt{\frac{f_d}{8}}U_d$. Hence, the comprehensive boundary shear stress τ_d can be expressed as

$$\tau_d=\rho\frac{f_d}{8}U_d^2, \tag{8}$$

where f_d represents the Darcy–Weisbach comprehensive friction factor.

Eq. (6) can only be solved numerically due to the influence of the secondary flow term $\rho\frac{\partial H(UV)_d}{\partial y}$ (Rameshwaran and Shiono 2007). Some methods for simplifying the equation have been proposed to solve the equation analytically. The secondary flow term was ignored in Shiono and Knight (1989) to obtain analytical solutions but considered in many other instances, especially in compound channels (Ervine et al. 2000). The secondary flow is assumed to be the constant $\frac{\partial[H(UV)_d]}{\partial y}=\Gamma$ in Shiono and Knight (1991) and determined on the basis of experimental data in particular situations. Ervine et al. (2000) proposed $U=K_1U_d$ and $V=K_2U_d$; thus, $UV=K_1K_2U_d^2=KU_d^2$, while K was not considered as a constant in vertical directions (Yang et al. 2007). We adopted the approach in Liu et al. (2013b) to obtain $(UV)_d=\overline{K}U_d^2$. Therefore, the secondary flow term is expressed as follows:

$$\rho\frac{\partial H(UV)_d}{\partial y}=\rho\frac{\partial(H\overline{K}U_d^2)}{\partial y}, \tag{9}$$

where $\overline{K}$ is the depth-averaged secondary flow coefficient that varies with the roughness and geometry of the channel, $\overline{K}U_d^2$ is a value that can approximately describe the two-

dimensional mixing process consisting of a horizontal shear layer and the exchange of mass, energy, and momentum between vegetated and non-vegetated areas (Ervine et al. 2000).

Therefore, Eq. (1) is expressed as

$$\rho g H S_0 + \frac{\partial}{\partial y}[\rho(\frac{f_d}{8})^{1/2}\lambda H^2 U_d \frac{\partial U_d}{\partial y}] - \rho\frac{f_d}{8}U_d^2 - \frac{1}{2}\rho(C_d\beta A_v)h_c P_u^2 U_d^2 = \rho\frac{\partial(H\overline{K}U_d^2)}{\partial y}. \quad (10)$$

The blocking effect of the canopy, which is represented by the porosity δ, should be considered in addition to the drag force of the canopy. The porosity is related to the volume density of the canopy. The effect of porosity should be considered for all terms, except the drag force term. Thus, Eq. (10) can be rewritten as

$$\delta\rho g H S_0 + \delta\frac{\partial}{\partial y}[\rho(\frac{f_d}{8})^{1/2}\lambda H^2 U_d \frac{\partial U_d}{\partial y}] - \delta\rho\frac{f_d}{8}U_d^2 - \frac{1}{2}\rho(C_d\beta A_v)h_c P_u^2 U_d^2 = \delta\rho\frac{\partial(H\overline{K}U_d^2)}{\partial y}. \quad (11)$$

Regions 1–4 are divided in Fig. 3 to illustrate the partition of the cross-section profile clearly. The interface between regions 1 and 2 is between vegetated and non-vegetated areas. The interface between regions 2 and 3 is located in the place where the depth-averaged streamwise velocity U_d reaches 95% of the maximum $U_{d\max}$, which we think that the mixing layer is fully developed. Region 4 considers the effect of the shore wall and is set up with its boundary located in the place where U_d reaches 95% of the maximum $U_{d\max}$. Two working conditions, namely, symmetrical and asymmetrical arrangements, are considered in this study. Only the diagram of the asymmetrical arrangement is selected for analysis because of the similarity of the region division in these two working conditions.

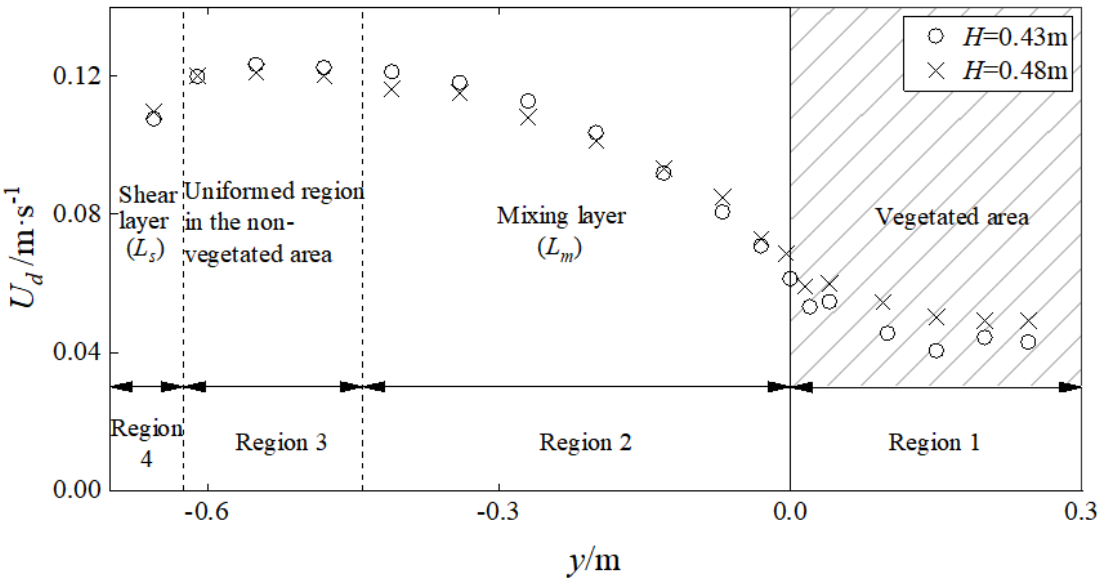

Fig. 3 Transverse distribution of depth-averaged streamwise velocity in the channel with the asymmetrical arrangement of FVIs

According to the division of the cross-section profile, the analytical solution to Eq. (11) can be derived as follows:

(1) For the vegetated area, namely, region 1 in Fig. 3, U_d is expressed as

$$U_d^{(1)} = (A_1 e^{\gamma_1 y} + A_2 e^{\gamma_2 y} + \omega_1)^{1/2}, \tag{12}$$

where $\gamma_1 = \frac{1}{H\lambda}(\frac{8}{f_d})^{1/2}\{\overline{K_1} + [\overline{K_1}^2 + \lambda(\frac{f_d}{8})^{1/2}(\frac{m}{\delta}C_d\beta D h_c P_u^2 + \frac{f_d}{4})^{1/2}\}$, $\gamma_2 = \frac{2}{H\lambda}(\frac{8}{f_d})^{1/2}\overline{K_4} - \gamma_1$,

$\omega_1 = \frac{gHS_0}{\frac{f_d}{8} + \frac{C_d\beta m D h_c P_u^2}{2\delta}}$, and A_1 and A_2 are unknown constants.

(2) For the non-vegetated area, namely, region 2, region 3, and region 4 in Fig. 3, U_d is expressed as

$$U_d^{(2)} = (A_3 e^{\gamma_3 y} + A_4 e^{\gamma_4 y} + \omega_2)^{1/2}, \tag{13}$$

where $\gamma_3 = \frac{1}{H\lambda}(\frac{8}{f_d})^{1/2}\{\overline{K_2} + [\overline{K_2}^2 + \lambda(\frac{f_d}{8})^{1/2}(\frac{f_d}{4})]^{1/2}\}, \gamma_4 = \frac{2}{H\lambda}(\frac{8}{f_d})^{1/2}\overline{K_2} - \gamma_3, \omega_2 = \frac{8gHS_0}{f_d}$,

and A_3 and A_4 are unknown constants.

$$U_d^{(3)} = (A_5 e^{\gamma_5 y} + A_6 e^{\gamma_6 y} + \omega_3)^{1/2}, \tag{14}$$

where $\gamma_5 = \frac{1}{H\lambda}(\frac{8}{f_d})^{1/2}\{\overline{K_3} + [\overline{K_3}^2 + \lambda(\frac{f_d}{8})^{1/2}(\frac{f_d}{4})]^{1/2}\}, \gamma_6 = \frac{2}{H\lambda}(\frac{8}{f_d})^{1/2}\overline{K_3} - \gamma_5, \omega_3 = \frac{8gHS_0}{f_d}$,

and A_5 and A_6 are unknown constants.

$$U_d^{(4)} = (A_7 e^{\gamma_7 y} + A_8 e^{\gamma_8 y} + \omega_4)^{1/2}, \tag{15}$$

where $\gamma_7 = \frac{1}{H\lambda}(\frac{8}{f_d})^{1/2}\{\overline{K_4} + [\overline{K_4}^2 + \lambda(\frac{f_d}{8})^{1/2}(\frac{f_d}{4})]^{1/2}\}, \gamma_8 = \frac{2}{H\lambda}(\frac{8}{f_d})^{1/2}\overline{K_4} - \gamma_7, \omega_4 = \frac{8gHS_0}{f_d}$,

and A_7 and A_8 are unknown constants.

Superscripts (1)–(4) of U_d represent regions 1–4 in Fig. 3, respectively. $\overline{K_1} - \overline{K_4}$ are the secondary flow coefficients in regions 1–4, respectively. f_d is the friction coefficient that will be specifically introduced in the later section. A_1–A_8 can be derived from the boundary conditions in the following section.

Boundary conditions for analytical solutions

The flow structure under two experimental conditions of symmetrical and asymmetric arrangements of FVIs is explored in this study. Diagrams of the two experimental conditions are shown in Fig. 4, where B is the width of the channel. Let αB and $(1-\alpha)B$ be the respective widths of vegetated and non-vegetated areas ($0 \le \alpha \le 1$) to simplify the calculation.

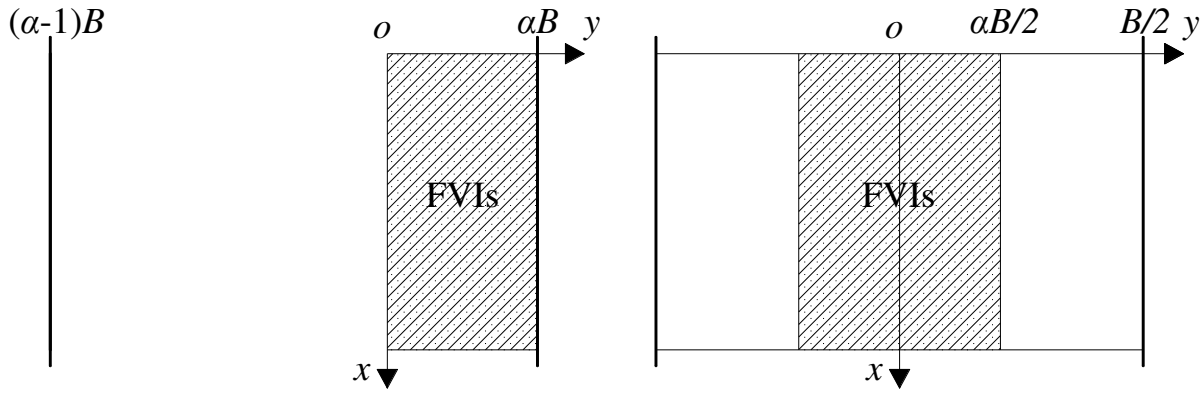

(a) Asymmetrical arrangement case (b) Symmetrical arrangement case

Fig. 4 Diagrams of the two arrangement cases

Using suitable boundary conditions to obtain unknown coefficients A_1–A_8 is necessary to obtain solutions of U_d for symmetric and asymmetric arrangements of FVIs.

(1) Boundary conditions for the asymmetrical arrangement of FVIs

a. $U_d^{(1)} = 0$ for $y = \alpha B$ is obtained by utilizing the no-slip boundary condition in the vegetated side.

b. $U_d^{(4)} = 0$ for $y = (\alpha - 1)B$ is obtained by applying the no-slip boundary condition in the non-vegetated side.

c. $U_d^{(i)} = U_d^{(i+1)}$ according to the continuity of depth-averaged streamwise velocity at the interface between two adjacent regions.

d. $\partial U_d^{(i)} / \partial y = \partial U_d^{(i+1)} / \partial y$ due to the continuity of velocity gradient at the interface between two adjacent regions.

(2) Boundary conditions of the symmetrical arrangement of FVIs

a. The velocity distribution is symmetrical along the centerline of the channel, and thus the velocity gradient at the center is equal to zero, such that $\partial U_d^{(1)} / \partial y = 0$ for $y = 0$.

b. $U_d^{(4)} = 0$ for $y = B/2$ is obtained by applying the no-slip boundary condition.

c. $U_d^{(i)} = U_d^{(i+1)}$ according to the continuity of depth-averaged streamwise velocity at the interface between two adjacent regions.

d. $\partial U_d^{(i)} / \partial y = \partial U_d^{(i+1)} / \partial y$ because of the continuity of velocity gradient at the interface between two adjacent regions.

Application principle and calibration coefficients

The lateral eddy viscosity coefficient λ, friction coefficient f_d, porosity δ, shape factor β, depth-averaged drag coefficient C_d, and secondary flow coefficient $\overline{K}$ must be determined to calculate the lateral velocity distribution in the channel with FVIs. The channel cross section is subdivided into different subregions and suitable secondary flow coefficients are applied to each subregion using Eqs. (12)–(15) to establish the lateral distribution model of U_d. Considering the symmetrical arrangement of FVIs, only half of the cross section ought to be explored, which is then divided into four sub-regions as narrated above as well as the entire cross section in the asymmetrical arrangement of FVIs.

1. Transverse eddy viscosity coefficient λ

A constant "standard" value of λ = 0.067 is introduced to the four subregions to simplify the calibration procedure and modeling process ($\lambda = \kappa/6 = 0.4/6 \approx 0.067$, where κ is the Karmen constant). Note that the change of λ slightly affects the results of the SKM for the open-channel flow. Therefore, only the secondary flow coefficient $\overline{K}$ must be calibrated to simulate the transverse distribution of the streamwise velocity (Knight and Abril 1996; Abril 1997; Tang and Knight 2008).

2. Friction coefficient f_d

The derived calculation formula of the comprehensive friction coefficient f_d mainly uses the relationship among the channel bed boundary shear stress τ_g, floating island boundary shear stress τ_c, and comprehensive boundary shear stress τ_d, which is expressed as $\tau_d = (\chi_g \tau_g + \chi_c \tau_c) / \chi_d$.

Assuming that $\tau_g = \rho \frac{f_g}{8} U_{d_g}^2$, $\tau_c = \rho \frac{f_c}{8} U_{d_c}^2$, and $\tau_d = \rho \frac{f_d}{8} U_d^2$, the following equation is obtained:

$$\chi_d f_d U_d^2 = \chi_g f_g U_{d_g}^2 + \chi_c f_c U_{d_c}^2, \tag{16}$$

where f_g and f_c are the Darcy–Weisbach friction factors of the channel bed and floating island, respectively; χ_g and χ_c represent dimensionless wetted perimeters of the channel bed per unit width and floating island per unit width, respectively; and χ_d is the dimensionless comprehensive wetted perimeter per unit width, $\chi_d = \chi_g + \chi_c$.

According to the relationship between the depth-averaged streamwise velocity in the canopy region and the depth-averaged streamwise velocity of the total water depth H in Eq. (5), $U_{d_c} = P_u U_d$. The depth-averaged streamwise velocity of the entire water depth $U_d = \frac{1}{H}\int_0^H U dz$ can be expressed using the depth-averaged streamwise velocity in the canopy region $U_{d_c} = \frac{1}{h_c}\int_{h_g}^H U dz$ and the depth-averaged streamwise velocity in the gap region $U_{d_g} = \frac{1}{h_g}\int_0^{h_g} U dz$, such that $HU_d = h_c U_{d_c} + h_g U_{d_g}$. Therefore, the relationship between U_{d_c} and U_{d_g} can be derived as follows

$$U_{d_c} / U_{d_g} = \frac{P_u}{1 + h_c / h_g} \Big/ (1 - \frac{P_u}{1 + h_g / h_c}) = P_u'. \tag{17}$$

Thus, Eq. (16) can be transformed into

$$f_d = \frac{\chi_g f_g (P_u / P_u')^2 + \chi_c f_c P_u^2}{\chi_d} = \frac{\chi_g f_g (P_u / P_u')^2 + \chi_c f_c P_u^2}{\chi_g + \chi_c}. \tag{18}$$

The expression of the friction coefficient is obtained by combining the commonly used Chezy formula with the Manning equation. Therefore, the friction coefficient of the channel bed and the floating island can be expressed as

$$f_g = \frac{8 g n_g^2}{R_g^{1/3}}, \tag{19}$$

$$f_c = \frac{8 g n_c^2}{R_c^{1/3}}, \tag{20}$$

where n_g and n_c represent Manning's roughness coefficients of the channel bed and the floating island, respectively, and R_g and R_c denote hydraulic radiuses of gap and canopy

regions, respectively. Similarly, depth-averaged streamwise velocities of these two regions are expressed using the Chezy and Manning equations as follows:

$$U_{d_g} = \frac{R_g^{2/3} J_g^{1/2}}{n_g}, \tag{21}$$

$$U_{d_c} = \frac{R_c^{2/3} J_c^{1/2}}{n_c}, \tag{22}$$

where J_g and J_c are hydraulic slopes of gap and canopy regions, respectively. Considering that the flow condition in this research is steady and uniform, there is $J_g = J_c$. Accordingly, $U_{d_c} = P_u' U_{d_g}$ is combined with Eqs. (21) and (22) to express the relationship between R_g and R_c as follows:

$$\frac{R_g}{R_c} = \frac{n_g^{3/2}}{P_u'^{3/2} n_c^{3/2}}. \tag{23}$$

Hence, the comprehensive hydraulic radius of the channel cross section R_d can be expressed as

$$R_d = \frac{A_d}{\chi_d} = \frac{A_g + A_c}{\chi_g + \chi_c} = \frac{A_g / \chi_g + (A_c / \chi_c)\chi_c / \chi_g}{1 + \chi_c / \chi_g} = \frac{n_g^{3/2} / (n_c^{3/2} P_u'^{3/2}) + \beta'}{1 + \beta'} R_c, \tag{24}$$

where A_g and A_c are areas of the gap and canopy regions, respectively; A_d is the area of the entire cross section, $A_d = A_g + A_c$; and β' is the ratio of χ_c to χ_g, $\beta' = \chi_c/\chi_g$. We obtain the following equation on the basis of Eq. (24):

$$R_c = \frac{1 + \beta'}{\frac{n_g^{3/2}}{n_c^{3/2} P_u'^{3/2}} + \beta'} R_d. \tag{25}$$

Thus, the comprehensive friction factor f_d can be expressed by substituting Eqs. (19) and (20) and (23)–(25) into Eq. (18) as follows:

$$f_d = \frac{8g}{\chi_g + \chi_c} \left[\frac{n_g^{3/2} P_u'^{-3/2} + \beta' n_c^{3/2}}{(1 + \beta') R_d} \right]^{1/3} \left(\chi_g P_u^2 P_u'^{-3/2} n_g^{3/2} + \chi_c P_u^2 n_c^{3/2} \right). \tag{26}$$

The comprehensive hydraulic radius for areas covered by floating islands is approximately equal to $h_g/2$. Thus, the comprehensive friction factor of the part of the floating island can be expressed as

$$f_d = \frac{8g}{\chi_g + \chi_c}\left[\frac{n_g^{3/2}P_u'^{-3/2} + \beta' n_c^{3/2}}{(1+\beta')h_g/2}\right]^{1/3}\left(\chi_g P_u^2 P_u'^{-3/2} n_g^{3/2} + \chi_c P_u^2 n_c^{3/2}\right). \quad (27)$$

The comprehensive hydraulic radius of the free water surface for free water surface areas is approximately equal to h_g. Thus, the comprehensive friction factor of the free water part can be expressed as

$$f_g = \frac{8g n_g^2 P_u^2 P_u'^{-2}}{h_g^{1/3}}. \quad (28)$$

3. Porosity δ

Porosity δ refers to the volume of pure water per unit water body in the case of vegetation and is expressed as

$$\delta = 1 - V_{vegetation}/V_{column}, \quad (29)$$

where $V_{vegetation}$ is the vegetation volume per unit vegetated area, $V_{vegetation} = \frac{1}{4}\pi m D^2 h_c$, and V_{column} is the volume of the water column for one water depth column per unit vegetated area, $V_{volume} = H$.

4. Shape factor β and drag coefficient C_d

The results of earlier studies showed that both the drag coefficient C_d and the shape factor β may be considered equal to 1.0 (Schlichting 1960; Stone and Shen 2002; James 2004; Armanini et al. 2005; Rameshwaran and Shiono 2007; Tanino and Nepf 2008; Sun and Shiono 2009; Liu et al. 2013b).

5. Secondary flow coefficient $\overline{K}$

The secondary flow coefficient $\overline{K}$ is calibrated empirically in the current study to obtain the most consistent one with the lateral depth-averaged flow velocity distribution of the experiment and thus considered the optimal $\overline{K}$.

Comparative analysis of results

The reliability and validity of the analytical model is verified using the experimental results. Parameters used for modeling in both cases are listed in Table 2. Figs. 5–7 show the analytical results of U_d for symmetrical and unsymmetrical cases with two different flow

depths. Fig. 5 illustrates that the analytical results of the symmetrical case with large width (b = 0.6 m) are consistent with the experimental results regardless of a high or low flow depth. The comparison of Figs. 5(a) and 5(b) shows that the velocity gradient $\partial U_d / \partial y$ at low water depth is larger than that at high water depth in the mixing layer. The rapid increase of U_d with large water depth to the maximum from the vegetated area to the non-vegetated area is consistent with engineering practice. The velocity in the non-vegetated area at low water depth is slightly larger than that at high water depth. Moreover, values of the secondary flow coefficient $\overline{K}$ remain nearly unchanged in the vegetated area (region 1) with the increase of water depths but increase from 0.9% to 1.2%, 2.5% to 5.0%, and 1.0% to 2.0% in regions 3, 4, and 5 of the non-vegetated area, respectively (Table 2).

Fig. 6 presents that the prediction of the model is also satisfactory in the symmetrical case with a small width (b = 0.3 m). Similar to the aforementioned case, U_d increases rapidly toward the maximum value at a low water depth and the maximum velocity value at low water depth slightly outweighs that at high water depth. However, some deviations exist between the symmetrical case with small width and that with large width. For example, values of the secondary flow coefficient $\overline{K}$ in region 1 in the small width case are one order of magnitude larger than those in the large width one and reach values at 0.5% and −1.0% for low and high water depths, respectively. This phenomenon is likely due to the weakened resistance of vegetation to secondary flows along with the decrease of the width of the vegetated area (region 1) that enlarges the secondary flow coefficient in that area. Moreover, values of the secondary flow coefficient $\overline{K}$ change from 0.5% to −1.0% as the water depth grows in the same region, thereby indicating the change in direction of the secondary flow's rotation, which is a different result from that of the large width case. Compared with the large width case, the velocity changes more gradually in the small width case due to the wider mixing layer.

The model can also successfully predict the lateral variation of depth-averaged streamwise velocity at low and high water depths for the asymmetrical case, as shown in Fig. 7. U_d alters more sharply at low water depth and the maximum value it reaches is larger than that at high water depth in the mixing layer. Moreover, negative signs of the secondary flow coefficient $\overline{K}$ are contrary to the symmetrical cases, as presented in Table 2. The distinctive arrangement of FVIs may alter flow patterns in symmetrical and asymmetrical cases and

cause this result. The modeled results are slightly smaller than the experimental data when 0.2 m < y < 0.3 m likely because the shore wall friction is neglected.

Table 2

Parameters used in modeling the open-channel flow through FVIs

Cases	λ_1	λ_2	λ_3	λ_4	$\overline{K_1}(\%)$	$\overline{K_2}(\%)$	$\overline{K_3}(\%)$	$\overline{K_4}(\%)$
Run 1	0.067	0.067	0.067	0.067	0.1	0.9	2.5	1.0
Run 2	0.067	0.067	0.067	0.067	0.0	1.2	5.0	2.0
Run 3	0.067	0.067	0.067	0.067	0.5	1.8	9.0	0.5
Run 4	0.067	0.067	0.067	0.067	−1.0	2.9	8.0	0.5
Run 5	0.067	0.067	0.067	0.067	−1.0	−3.0	−20.0	0.1
Run 6	0.067	0.067	0.067	0.067	−1.0	−3.2	−17.5	−0.2

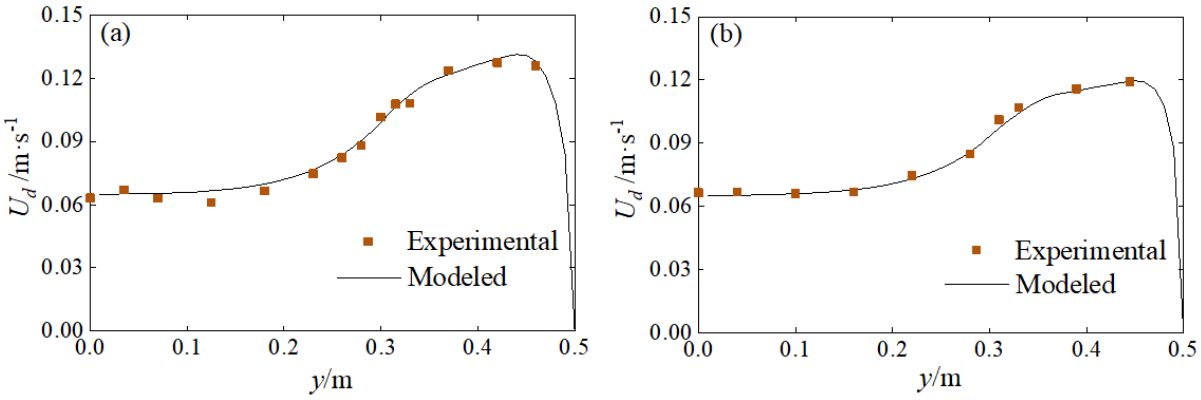

Fig. 5 Transverse variation of depth-averaged streamwise velocity U_d for the symmetrical arrangement of FVIs with wide width (b = 0.6 m) and two water depths of (a) H = 0.43 m, Run 1 and (b) H = 0.48 m, Run 2

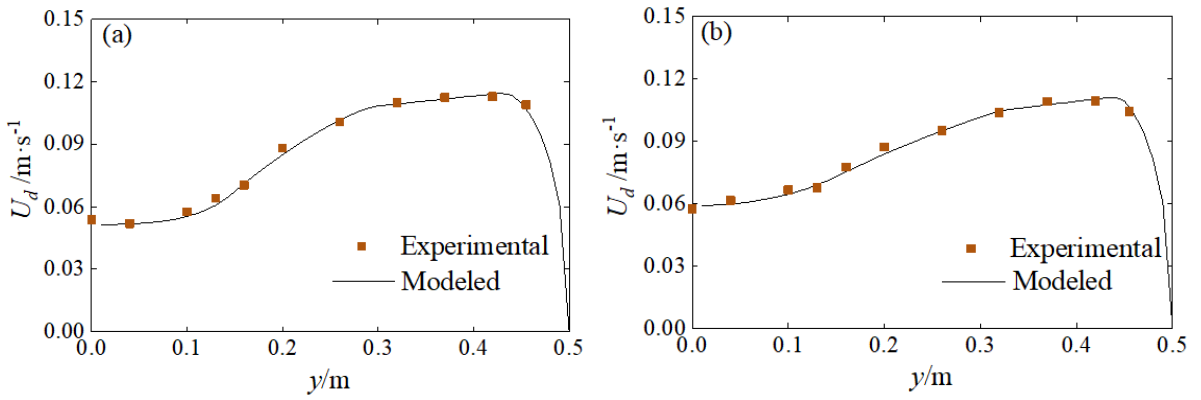

Fig. 6 Transverse variation of depth-averaged streamwise velocity U_d for the symmetrical arrangement of FVIs with narrow width (b = 0.3 m) and two water depths of (a) H = 0.43 m, Run 3 and (b) H = 0.48 m, Run 4

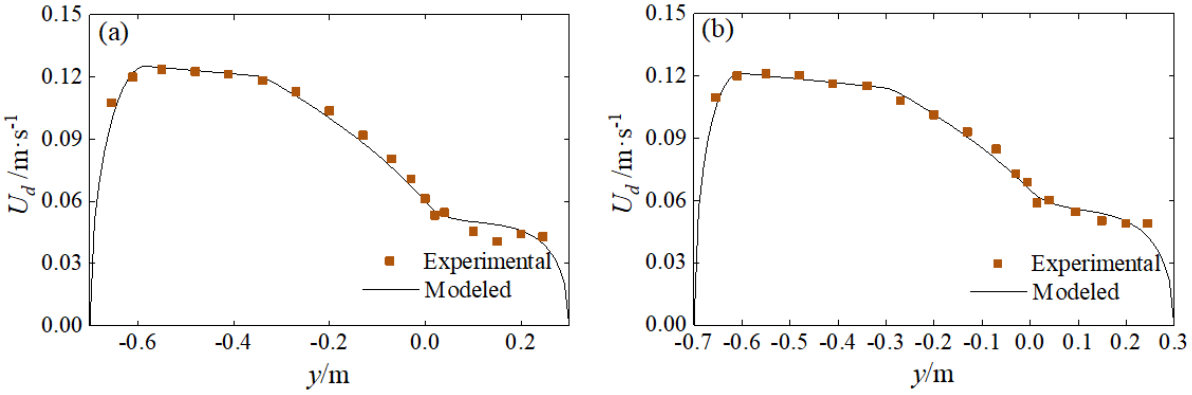

Fig. 7 Transverse variation of depth-averaged streamwise velocity U_d for the asymmetrical arrangement of FVIs with two water depths of (a) H = 0.43 m, Run 5 and (b) H = 0.48 m, Run 6

Error statistics, including the calculation of average absolute error $\overline{\varepsilon_a}$ and average relative error $\overline{\varepsilon_r}$ are carried out to compare the model results with the measured data, as shown in Table 3. The absolute error is expressed as

$$\varepsilon_a = (U_d)_{computed} - (U_d)_{measured}, \tag{30}$$

where subscripts "computed" and "measured" represent computed and measured values of U_d, respectively. The average absolute error based on Eq. (30) is calculated as

$$\overline{\varepsilon_a} = \frac{1}{N}\sum_{i=1}^{N} abs(\varepsilon_{ai}), \tag{31}$$

where N represents the number of measuring perpendiculars in the cross section for each case.

The relative error ε_r based on Eq. (30) is expressed as

$$\varepsilon_r = \frac{\varepsilon_a}{(U_d)_{measured}}, \tag{32}$$

and the average relative error $\overline{\varepsilon_r}$ is expressed as

$$\overline{\varepsilon_r} = [\frac{1}{N}\sum_{i=1}^{N} abs(\varepsilon_{ri})]\times 100\%. \tag{33}$$

Table 3 presents that the prediction results of U_d are reliable, the average absolute errors are within 0.004 m/s, and the peak of the maximum average absolute error $\overline{\varepsilon_a}$ of Run 5 case is at 0.0031 m/s. Average relative errors vary from 1.99% to 4.74%. The prediction result of the Run 2 case is the most accurate among all the cases, with minimum values of $\overline{\varepsilon_a}$ and $\overline{\varepsilon_r}$ equal to 0.0022 m/s and 2.30%, respectively. The model can appropriately predict the depth-averaged streamwise velocity according to error statistics.

Table 3

Error statistics of depth-averaged streamwise velocities for all cases

Cases	Run 1	Run 2	Run 3	Run 4	Run 5	Run 6
Average absolute error (m/s) $\overline{\varepsilon_a}$	0.0025	0.0022	0.0016	0.0016	0.0031	0.0022
Average relative error (%) $\overline{\varepsilon_r}$	3.10	2.30	2.12	1.99	4.74	3.14

Sensitive analyses of secondary flow coefficients of symmetrical and asymmetrical cases at a water depth of H = 0.43 m are performed to determine their influence on the transverse variation of U_d and signs of $\overline{K}$, as shown in Fig. 8. Three conditions are considered for each case in this study. $\overline{K_1}=\overline{K_2}=\overline{K_3}=\overline{K_4}=0$, $\overline{K_1}=1\%, \overline{K_2}=1\%, \overline{K_3}=1\%, \overline{K_4}=1\%$, and $\overline{K_1}=-1\%, \overline{K_2}=1\%, \overline{K_3}=1\%, \overline{K_4}=1\%$ are adopted for the symmetrical case. $\overline{K_1}=\overline{K_2}=\overline{K_3}=\overline{K_4}=0$, $\overline{K_1}=-2\%, \overline{K_2}=-2\%, \overline{K_3}=-20\%, \overline{K_4}=-0.2\%$, and $\overline{K_1}=-2\%, \overline{K_2}=-2\%, \overline{K_3}=20\%, \overline{K_4}=-0.2\%$ are applied for the asymmetrical case. Other coefficients not mentioned in this section remain stable, as shown in the aforementioned sections. Fig. 8 shows that errors of both cases between the analysis and experimental results are large when the secondary flow is ignored. Hence, the secondary flow must be considered. The results obtained are inaccurate compared with the analysis results, which are relatively close to numerical values adopted in this study, when the sign of only one coefficient is changed and the sign and size of the three other coefficients remain unchanged (signs of $\overline{K_1}$ and $\overline{K_3}$ are changed in this study for symmetrical and asymmetrical cases, respectively). The results obtained are satisfactory only when signs of second flow coefficients $\overline{K}$ remain stable with those presented in Table 2. Hence, secondary flow coefficient symbols used in this study are appropriate.

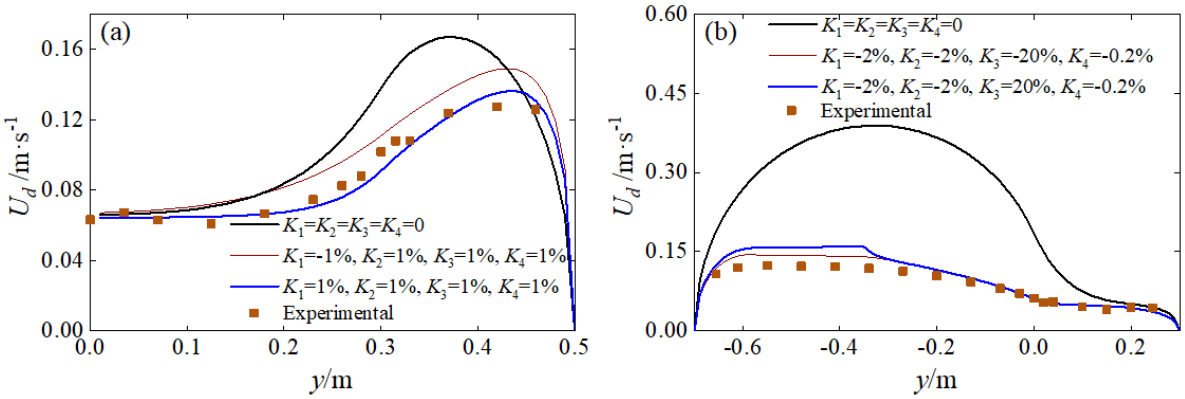

Fig. 8 Influence of the secondary flow on the transverse variation of U_d for symmetrical and asymmetrical cases at a water depth of H = 0.43m: (a) Run 1 (b) Run 5

Conclusions

The lateral distribution of depth-averaged streamwise velocity for the steady uniform flow in the open channel with symmetrical and asymmetrical arrangements of FVIs based on the N–S equation is explored in this study. The canopy drag force is added to the N–S equation as the additional resistance term, and the governing equation is solved with suitable boundary conditions. The cross section is divided into four calculation regions according to flow characteristics and the model layout. Calculation methods of six necessary parameters utilized in each region, namely, lateral eddy viscosity coefficient λ, friction coefficient f_d, porosity δ, shape factor β, drag coefficient C_d, and secondary flow coefficient $\overline{K}$, are discussed in detail. The secondary flow coefficient $\overline{K}$ plays an important role in the prediction of the lateral distribution of depth-averaged streamwise velocity. If the effect of the secondary flow is neglected, then predicting depth-averaged velocities of the open-channel flow with FVIs is difficult. Analytical solutions of the lateral distribution of depth-averaged velocities are presented for symmetrical and asymmetrical cases. The consistency between the calculated results of the theoretical solution and experimental data indicated that the model can effectively predict the lateral distribution of the depth-averaged streamwise velocity in the open-channel flow with FVIs.

Although some theoretical results have been obtained using the proposed analytical model, the universality of these theoretical results requires further investigations. Meanwhile, limitations exist in the proposed analytical model (i.e., Eqs. (12)–(15)). The analytical model is unsuitable and infeasible when the flow state fails to satisfy the steady uniform flow

condition. Moreover, model parameters need to be modified under different experimental conditions and additional work is needed to provide detailed references.

Nomenclature

The following symbols are used in this study:

A_1–A_8 = Integration constants in Eqs. (12)–(15)

A_v = Projected area of canopy per unit volume in the longitudinal direction (m^{-1})

A_d = Area of the entire cross section (m^2)

b = Width of floating vegetated islands (m)

B = Flume width (m)

C_b = Bed friction coefficient (-)

C_d = Drag force coefficient (-)

D = Canopy diameter (m)

f_d = Darcy–Weisbach comprehensive friction factor (-)

F_v = Drag force, as defined by Eq. (2) (N/m^3)

g = Gravitational acceleration (m/s^2)

h_c = Height of the root canopy (m)

h_g = Height of the gap region (m)

H = Flow depth (m)

$\overline{K}$ = Secondary flow coefficient (-)

m = Number of columns per bed area (m^{-2})

n = Manning's roughness coefficient (-)

P_u = Scale parameter between U_{d_c} and U_d (-)

P_u' = Scale parameter between U_{d_c} and U_{d_g} (-)

Q = Flow rate (m^3/s)

R = Hydraulic radius (m)

S_0 = Channel bed slope (-)

u', v', w' = Fluctuating velocities in x, y, and z directions (m/s)

U_d = Depth-averaged streamwise velocity (m/s)

U_{d_c} = Depth-averaged streamwise velocity in the canopy region (m/s)

U_{d_g} = Depth-averaged streamwise velocity in the gap region (m/s)

U_* = Local shear velocity (m/s)

V_{column} = Volume of the water depth column per unit vegetated bottom area (m)

$V_{vegetation}$ = Volume occupied by the vegetation per unit vegetated bottom area (m)

x, y, z = Streamwise, lateral, and vertical directions (-)

α = Coefficients in Eq. (5) (-)

β = Shape factor (-)

δ = Porosity (-)

λ = Lateral dimensionless eddy viscosity (-)

κ = Karman constant (-)

γ_{1-8}, w_{1-4} = Coefficients in Eqs. (12)–(15)

τ_{yx}, τ_{zx} = Reynolds shear stresses on planes perpendicular to y- and z-directions, respectively (N/m^2)

$\overline{\tau_{yx}}$ = Depth-averaged Reynolds shear stresses on planes perpendicular to the y-direction (N/m^2)

τ_d = Boundary shear stress (N/m^2)

χ = Dimensionless wetted perimeter per unit width (-)

$\overline{\varepsilon_{yx}}$ = Depth-averaged eddy viscosity (m^2/s)

g, c = Abbreviations of lower gap and upper canopy regions

Declarations

Acknowledgements The authors gratefully acknowledge their family, teachers, and classmates for their help in making this study more meaningful.

Data availability The datasets used or analyzed during the current study are available from the corresponding author on reasonable request.

Author contribution Wenxin Huai proposed the idea of this study. Xuecheng Fu did the majority of calculations, writing and editing. Feifei Wang revised the manuscript. The experiment was designed by Wenxin Huai and Mengyang Liu, and performed by Xuecheng Fu and Feifei Wang. All authors read and approved the final manuscript.

Funding This work was financially supported by the National Natural Science Foundation of China [grant numbers 52020105006 and 11872285].

Ethics approval and consent to participate Not applicable.

Consent for publication Not applicable.

Competing interests The authors declare that they have no competing interests.

References

Abril JB (1997) Numerical modelling of turbulent flow, sediment transport and flood routing using the finite element method. Dissertation, University of Birmingham

Armanini A, Righetti M, Grisenti P (2005) Direct measurement of vegetation resistance in prototype scale. J Hydraul Res 43(5):481–487. https://doi.org/10.1080/00221680509500146

Billore SK, Sharma JK (2009) Treatment performance of artificial floating reed beds in an experimental mesocosm to improve the water quality of river Kshipra. Water Sci Technol 60(11):2851–2859. https://doi.org/10.2166/wst.2009.731

Bonakdari H (2012) Establishment of relationship between mean and maximum velocities in narrow sewers. J Environ Manage 113:474–480. https://doi.org/10.1016/j.jenvman.2012.10.016

Chen G, Huai WX, Han J, Zhao MD (2010) Flow structure in partially vegetated rectangular channels. J Hydrodyn 22(4):590–597. https://doi.org/10.1016/S1001-6058(09)60092-5

Chua LH, Tan SB, Sim CH, Goyal MK (2012) Treatment of baseflow from an urban catchment by a floating wetland system. Ecol Eng 49:170–180. https://doi.org/10.1016/j.ecoleng.2012.08.031

Devi K, Khatua KK (2016) Prediction of depth averaged velocity and boundary shear distribution of a compound channel based on the mixing layer theory. Flow Meas Instrum 50:147–157. https://doi.org/10.1016/j.flowmeasinst.2016.06.020

Downing-Kunz M, Stacey M (2011) Flow-induced forces on free-floating macrophytes. Hydrobiologia 671(1):121–135. https://doi.org/10.1007/s10750-011-0709-1

Ervine DA, Babaeyan-Koopaei K, Sellin RHJ (2000) Two-dimensional solution for straight and meandering overbank flows. J Hydraul Eng 126(9):653–669. https://doi.org/10.1061/(ASCE)0733-9429(2000)126:9(653)

Fernandes JN, Leal JB, Cardoso AH (2014) Improvement of the lateral distribution method based on the mixing layer theory. Adv Water Resour 69(4):159–167. https://doi.org/10.1016/j.advwatres.2014.04.003

Huai WX, Xu ZG, Yang ZH, Zeng YH (2008) Two dimensional analytical solution for a partially vegetated compound channel flow. Appl Math Mech 29(8):1077–1084. https://doi.org/10.1007/s10483-008-0811-y

Huai WX, Gao M, Zeng YH, Li D (2009) Two-dimensional analytical solution for compound channel flows with vegetated floodplains. Appl Math Mech 30(9):1121–1130. https://doi.org/10.1007/s10483-009-0906-z

Huai WX, Geng C, Zeng YH, Yang ZH (2011) Analytical solutions for transverse distributions of stream-wise velocity in turbulent flow in rectangular channel with partial vegetation. Appl Math Mech (Engl Ed) 32(4):459–468. https://doi.org/10.1007/s10483-011-1430-6

Hwang L, LePage BA (2011) Floating islands—An alternative to urban wetlands. In: Wetlands. Springer, Dordrecht, pp 237–250

Huai WX, Wang W, Zeng YH (2013) Two-layer model for open channel flow with submerged flexible vegetation. J Hydraul Res 51(6):708–718. https://doi.org/10.1080/00221686.2013.818585

Huai W, Li C (2016) Longitudinal dispersion in open channel flow with suspended canopies. Water Sci Technol 74(3):722–728. https://doi.org/10.2166/wst.2016.236

James CS, Birkhead AL, Jordanova AA, O'Sullivan JJ (2004) Flow resistance of emergent vegetation. J Hydraul Res 42(4):390–8. https://doi.org/10.1080/00221686.2004.9728404

Knight DW, Abril JB (1996) Refined calibration of a depth-averaged model for turbulent flow in a compound channel. Proceedings of the Institution of Civil Engineers-Water Maritime and Energy 118(3):151–159. https://doi.org/10.1680/iwtme.1996.28682

Liu C, Luo X, Liu X, Yang K (2013b) Modeling depth-averaged velocity and bed shear stress in compound channels with emergent and submerged vegetation. Adv Water Resour 60:148–159. https://doi.org/10.1016/j.advwatres.2013.08.002

Liu C, Shan YQ, Yang KJ, Liu XN (2013a) The characteristics of secondary flows in compound channels with vegetated floodplains. J Hydrodyn 25:422–429. https://doi.org/10.1016/S1001-6058(11)60381-9

Liu C, Shan YQ, Lei JR, Nepf HM (2019) Floating treatment islands in series along a channel: the impact of island spacing on the velocity field and estimated mass removal. Adv Water Resour 129:222–231. https://doi.org/10.1016/j.advwatres.2019.05.011

532 Nahlik AM, Mitsch WJ (2006) Tropical treatment wetlands dominated by free-floating
533 macrophytes for water quality improvement in Costa Rica. Ecol Eng 28(3):246–257.
534 https://doi.org/10.1016/j.ecoleng.2006.07.006
535 Plew DR (2011) Depth-averaged drag coefficient for modeling flow through suspended
536 canopies. J Hydraul Eng 137(2):234–247. https://doi.org/10.1061/(ASCE)HY.1943-
537 7900.0000300
538 Rameshwaran P, Shiono K (2007) Quasi two-dimensional model for straight overbank flows
539 through emergent vegetation on floodplains. J Hydraul Res 45(3):302–315.
540 https://doi.org/10.1080/00221686.2007.9521765
541 Schlichting H (1960) Boundary layer theory. McGraw-Hill, New York
542 Shiono K, Knight DW (1991) Turbulent open-channel flows with variable depth across the
543 channel. J Fluid Mech 222(1):617–646. https://doi.org/10.1017/S0022112091001246
544 Stone BM, Shen HT (2002) Hydraulic resistance of flow in channels with cylindrical
545 roughness. J Hydraul Eng 128(5):500–6. https://doi.org/10.1061/(ASCE)0733-
546 9429(2002)128:5(500)
547 Sun X, Shiono K (2009) Flow resistance of one-line emergent vegetation along the floodplain
548 edge of a compound open channel. Adv Water Resour 32(3):430–438.
549 https://doi.org/10.1016/j.advwatres.2008.12.004
550 Tanner CC, Headley TR (2011) Components of floating emergent macrophyte treatment
551 wetlands influencing removal of stormwater pollutants. Ecol Eng 37(3):474–486.
552 https://doi.org/10.1016/j.ecoleng.2010.12.012
553 Tang X; Knight DW (2008) Lateral depth-averaged velocity distributions and bed shear in
554 rectangular compound channels. J Hydraul Eng 134(3):1337–1342.
555 https://doi.org/10.1061/(ASCE)0733-9429(2008)134:9(1337)
556 Tanino Y, Nepf HM (2008) Laboratory investigation of mean drag in a random array of rigid,
557 emergent cylinders. J Hydraul Eng 134(1):34–41. https://doi.org/10.1061/(ASCE)0733-
558 9429(2008)134:1(34)
559 White BL, Nepf HM (2008) A vortex-based model of velocity and shear stress in a partially
560 vegetated shallow channel. Water Resour Res 44(1):1–15.
561 https://doi.org/10.1029/2006WR005651

562 Wang FF, Huai WX, Liu MY, Fu XC (2020) Modeling depth-averaged streamwise velocity in
563 straight trapezoidal compound channels with ice cover. J Hydrodyn 585:123446.
564 https://doi.org/10.1016/j.jhydrol.2019.124336

565 Yang KJ, Cao SY, Knight DW (2007) Flow patterns in compound channels with vegetated
566 floodplains. J Hydraul Eng 133(2):148–159. https://doi.org/10.1061/(ASCE)0733-
567 9429(2007)133:2(148)

568 Zhong Y, Huai WX, Chen G (2019) Analytical model for lateral depth-averaged velocity
569 distributions in rectangular Ice-Covered channels. J Hydraul Eng 145(1):04018080.
570 https://doi.org/10.1061/(ASCE)HY.1943-7900.0001557

Figures

Figure 1

Global view of the channel with different FVI arrangements

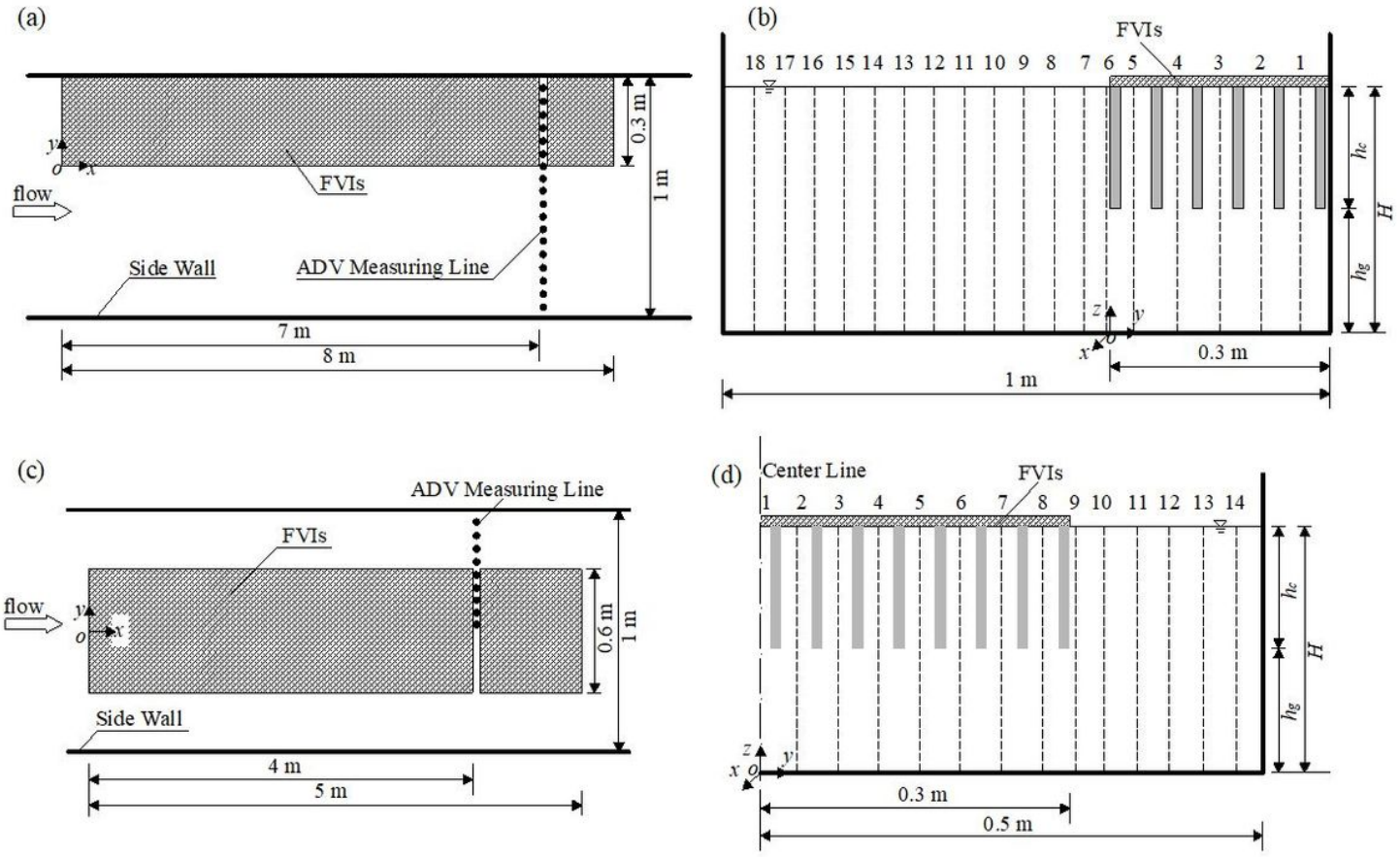

Figure 2

Diagrams of the FVI layout in the laboratory flume: (a) Top view of the asymmetrical arrangement case; (b) Cross-section profile of the asymmetrical arrangement case; (c) Top view of the symmetrical arrangement case; (d) Cross-section profile of the symmetrical arrangement case with the canopy height hc, gap height hg, and water depth H

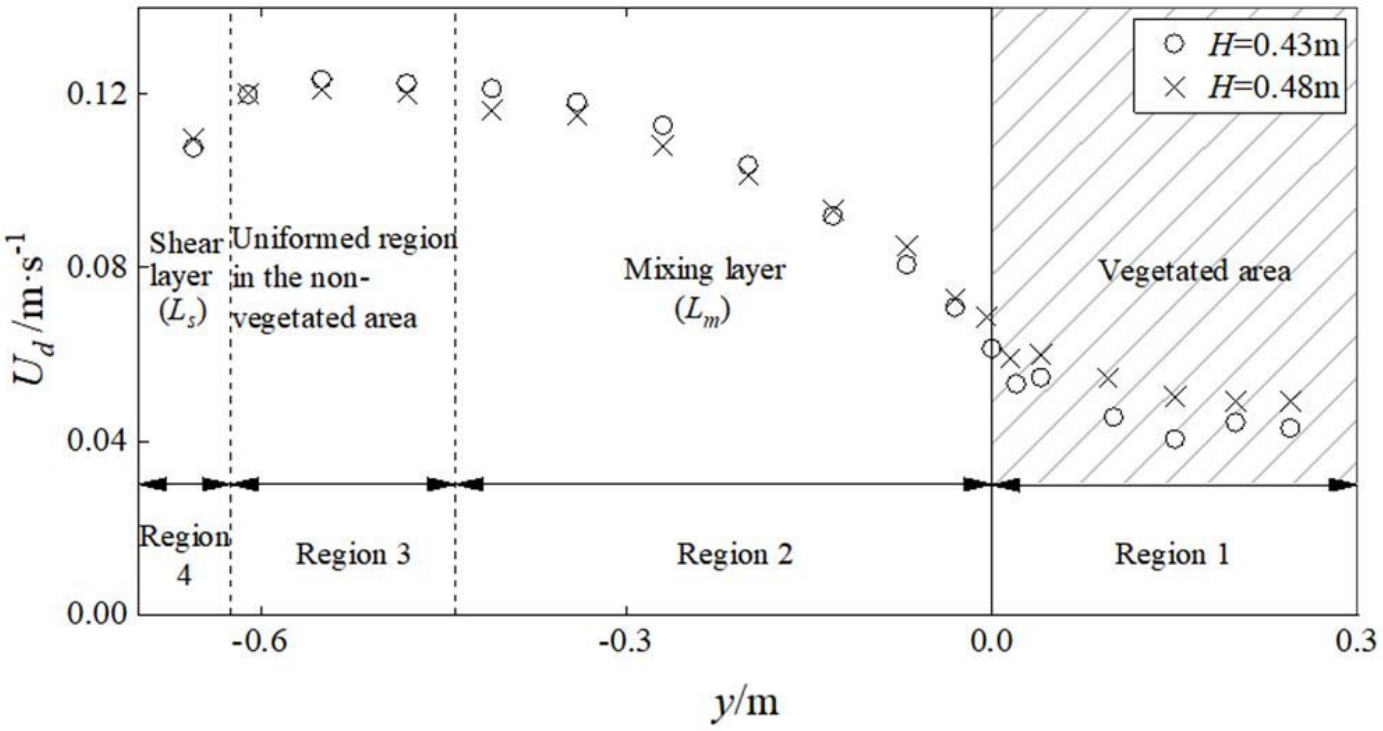

Figure 3

Transverse distribution of depth-averaged streamwise velocity in the channel with the asymmetrical arrangement of FVIs

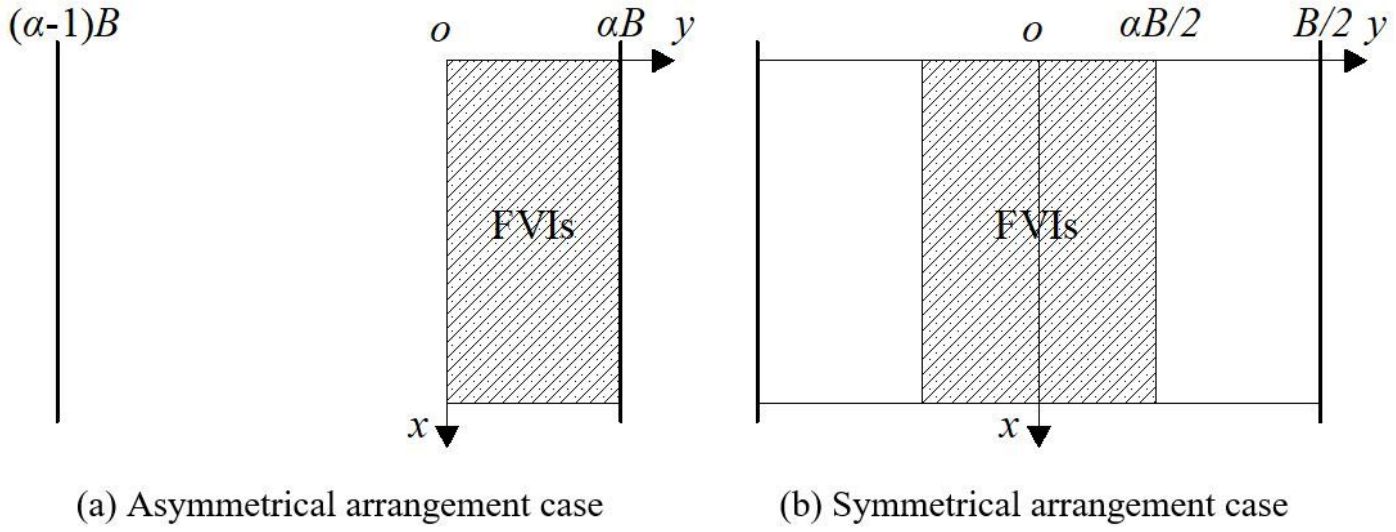

(a) Asymmetrical arrangement case (b) Symmetrical arrangement case

Figure 4

Diagrams of the two arrangement cases

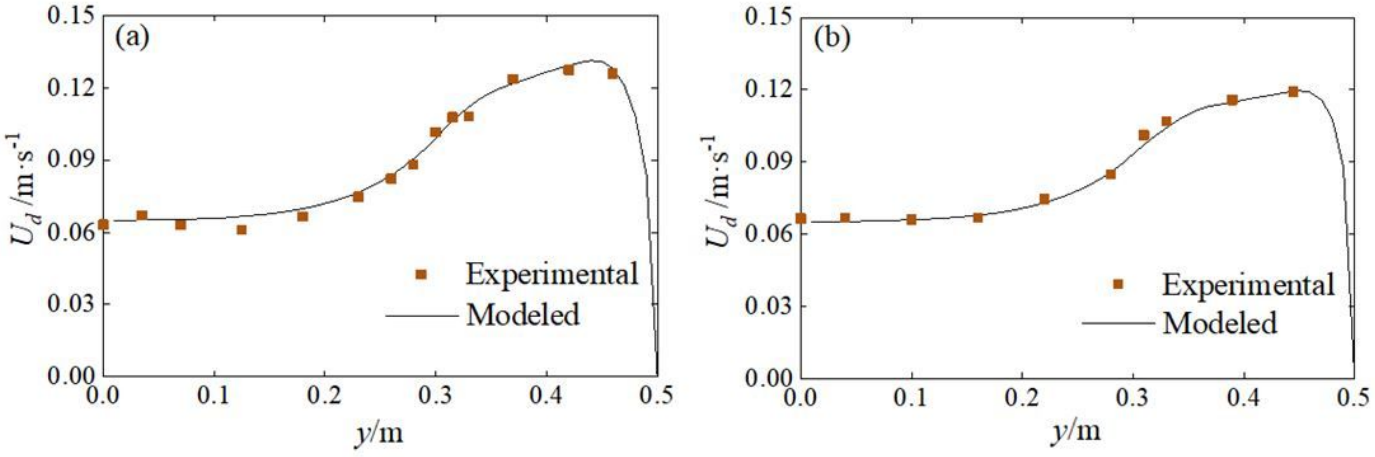

Figure 5

Transverse variation of depth-averaged streamwise velocity Ud for the symmetrical arrangement of FVIs with wide width (b = 0.6 m) and two water depths of (a) H = 0.43 m, Run 1 and (b) H = 0.48 m, Run 2

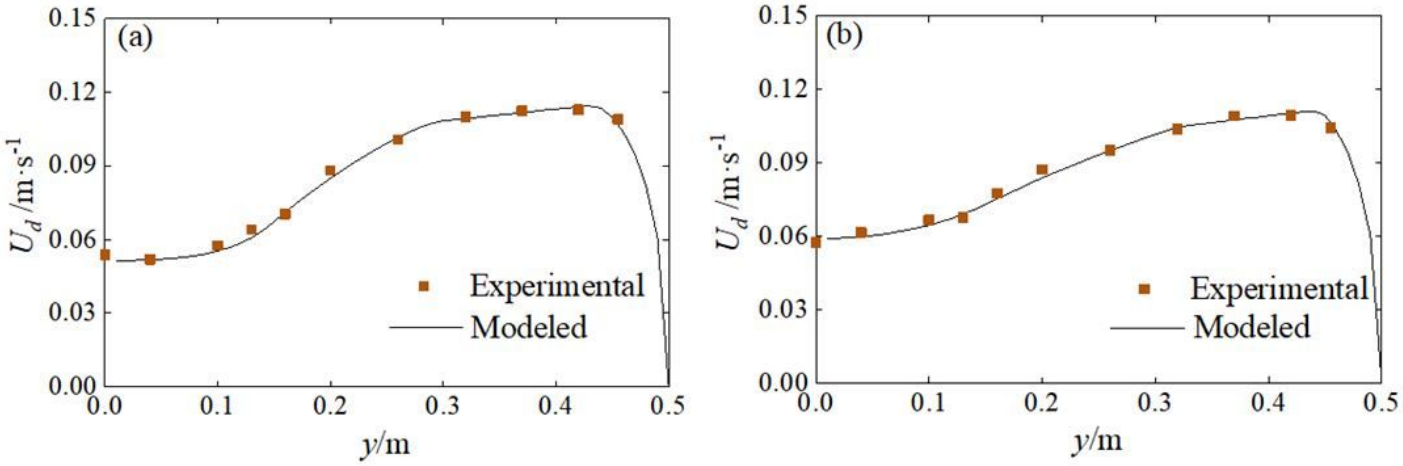

Figure 6

Transverse variation of depth-averaged streamwise velocity Ud for the symmetrical arrangement of FVIs with narrow width (b = 0.3 m) and two water depths of (a) H = 0.43 m, Run 3 and (b) H = 0.48 m, Run 4

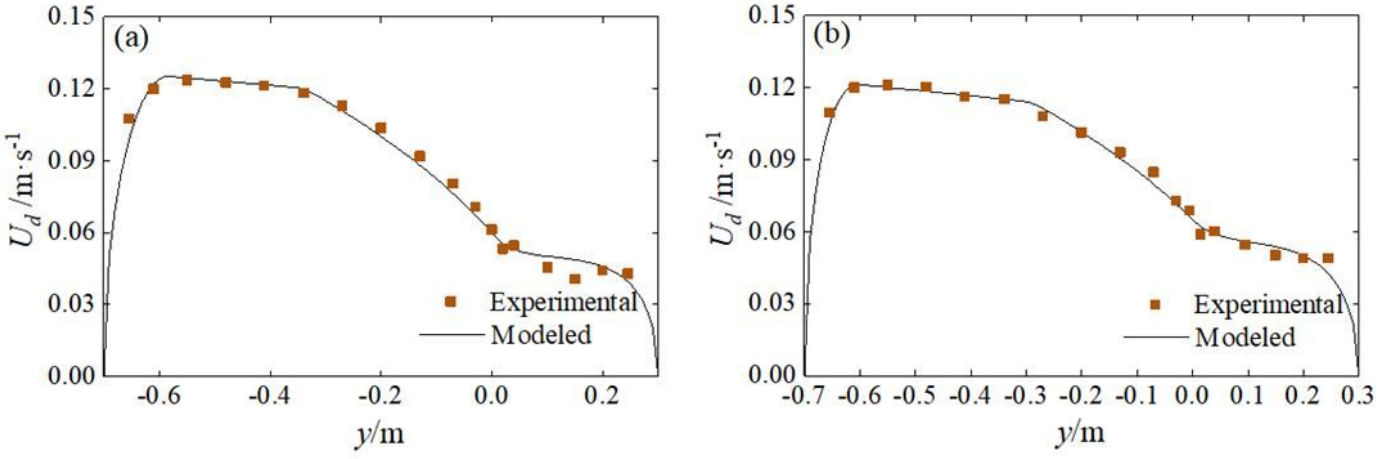

Figure 7

Transverse variation of depth-averaged streamwise velocity Ud for the asymmetrical arrangement of FVIs with two water depths of (a) H = 0.43 m, Run 5 and (b) H = 0.48 m, Run 6

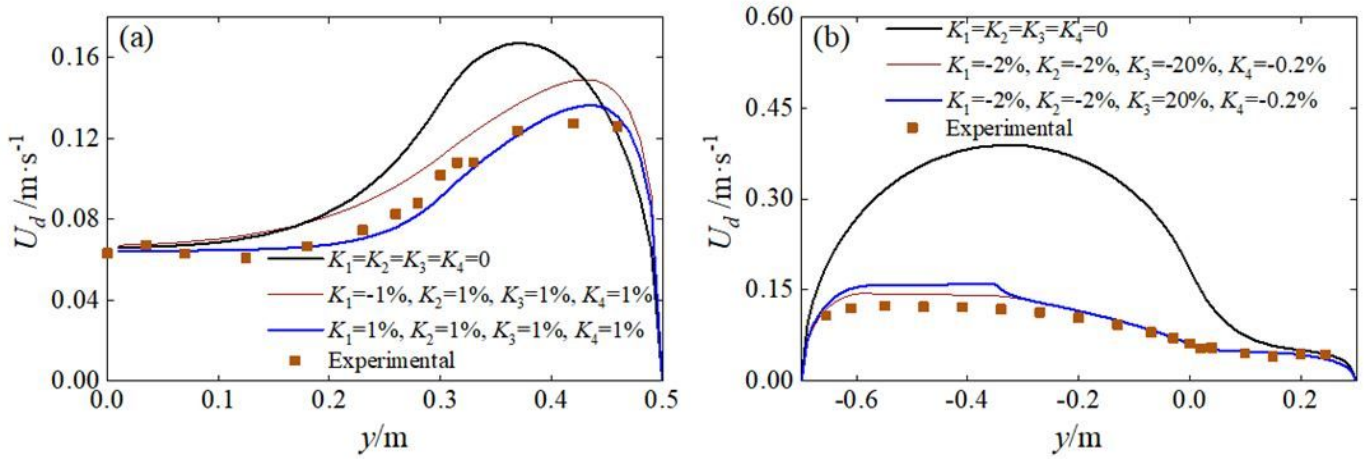

Figure 8

Influence of the secondary flow on the transverse variation of Ud for symmetrical and asymmetrical cases at a water depth of H = 0.43m: (a) Run 1 (b) Run 5